Supporting Information

Akiva-Tal et al. 10.1073/pnas.1102608108

SI Text

Materials. Phosphoenolpyruvate (PEP), EGTA, D_2O, and HCl were purchased from Sigma-Aldrich. Citric acid was purchased from Frutarom. Triphenylphosphine PPh_3 was purchased from Fluka.

All chemicals were used as purchased. Stock solution of 0.5 M EGTA was prepared by dissolving 9.50 gr EGTA in 50 mL H_2O.

A stock solution of 0.5 M PPh_3 was prepared by dissolving 0.655 gr in 5 mL of $CHCl_3$. Capillary tubes were filled with 50(±2) μL of PPh_3 stock solution and sealed with UV glue. For quantitative solution NMR measurements such a capillary was inserted to the NMR tubes.

EGTA:Ca^{2+} solution was prepared by dissolving into the EGTA solution $CaCO_3$ to its solubility limit.

Identification and Quantification of PEP, Citrate, and Inorganic Phosphate (Pi) by Solution NMR. Two abundant metabolites, PEP and citrate, and inorganic phosphate were found in the "soluble fraction" of the gastrolith. Herein we describe the analytic pathway employed to establish their identification and quantify their levels.

1. 1D ^1H NMR spectra—Fig. S1. The most intense peaks in the gastrolith-EGTA spectrum (Fig. S1*b*) are EGTA peaks, identical to the EGTA peaks in the reference spectrum (Fig. S1*a*). In addition, two proton multiplets are detected in spectrum (Fig. S1*b*): the geminally coupled proton pair of PEP and the AB pair of citrate shown in enlargement. The gastrolith-HCl spectrum (Fig. S1*c*) clearly reports the same peaks of the two metabolites, PEP and citrate. Variations in the CH_2 multiplets observed between the two spectra arise from differences in the pH between the two solutions. Their values, reported in Table S1, are in agreement with literature values as reported in the human metabolome database [HMDB00263 PEP; HMDB00094 citrate] (1–3) The reproduction of the same soluble gastrolith content with the HCl preparatory method further substantiates the identification of the metabolites under simplified spectral conditions.

2. Establishing connectivities within the two metabolites—Fig. S2. ^1H-^1H correlation (COSY), ^1H-^{31}P heteronuclear multiple-bond coherence (HMBC), and ^1H-^{13}C heteronuclear single quantum coherence (HSQC) spectra establish the connectivities with the two metabolites, hence solidify PEP and citrate assignments as the major organic molecules within the gastrolith soluble fraction.

3. Chemical identity confirmation via spiking—Fig. S3. Identical spiking experiments carried out with the gastrolith-EGTA solution (not shown) gave the same results, and thus similarly confirmed the chemical identification.

The above solution NMR experiments provide unequivocal evidence for the presence of Pi, PEP, and citrate within the soluble fraction of the gastroliths. These are clearly identified as the most abundant molecules.

4. Pi, PEP, and citrate levels: Quantitative solution NMR. The solution NMR spectra serve to quantitatively determine the abundance and variance of the above identified molecules in a representative set of gastroliths. A sealed PPh_3 capillary was placed in the NMR tube and served as internal quantitative standard whose integrated ^{31}P peak intensity represents 25 μmol P. The integrated peak intensities of Pi and PEP served to determine their mole levels within the NMR tube.

A quantitative ^1H NMR spectrum was recorded. Citrate level (in the NMR tube) was determined by comparison of its integrated proton peak intensity to that of PEP. In cases where the PEP levels were too low for accurate determination, the integrated peak intensities between two different samples were compared.

For the soluble fraction fully relaxed 161.3 MHz ^{31}P and 400 MHz ^1H solution NMR spectra were recorded under the same preparation conditions using 20-s and 1-s repetition delays, respectively. Mole amounts of Pi, PEP, and citrate in the NMR tube were corrected to account for the full volume of each soluble fraction.

To evaluate the Pi/Ca and PEP/Ca mol % the following assumptions were employed:

The gastrolith soluble matrix weight is taken as 90% of its total weight to account for approximately 10% of its insoluble matrix.

We assume that all Pi (PO_4^{3-}) is charge balanced by Ca^{2+} ions, implying a stoichiometric ratio of $Ca_3(PO_4)_2$. The total weight of this "compound" was calculated using the determined number of moles of Pi and then subtracted from the soluble fraction weight. Likewise, the weights of PEP and citrate (known from the determined number of moles) were also subtracted. The remaining weight is attributed to $CaCO_3 \cdot H_2O$ [molecular weight (MW) = 118.1 gr/mol] accounting for the known 1:1 stoichiometry of stable amorphous calcium carbonate (ACC). Summation of the number of moles of Ca in $CaCO_3$ and $Ca_3(PO_4)_2$ yields the total number of moles in the soluble fraction from which the desired mol % are derived. Accounting for the accumulated experimental errors, the estimated accuracy of the determined mole ratios is 20–30%. A representative set of mole ratios as obtained for nine different gastroliths is shown in Table S2.

Analyses of Solid State NMR Experimental Results. *$^{13}C\{^{31}P\}$ REDOR (rotational-echo double-resonance) analysis and implications.* The $^{13}C\{^{31}P\}$ REDOR dipolar recoupling technique enables selective identification of carbon species, ACC carbonates, or any other bioorganic species, with adjacent phosphorus moieties. This experiment is performed in two steps: first, without dipolar recoupling, producing a reference spectrum, S_0, with all ^{13}C species reported; second, reintroducing dipolar coupling with ^{31}P nuclei, producing the recoupled S_R spectrum. In the latter, peaks of carbon species with proximate ^{31}P atoms, up to 9 Å apart, are attenuated compared to the reference spectrum. This attenuation of spectral peaks enables (*i*) spectral editing capability often manifested by the difference spectrum, $\Delta S = S_0 - S_R$, exclusively exhibiting peaks of ^{13}C species with adjacent ^{31}P moieties (4, 5), and (*ii*) geometrical information by determination of the dipolar coupling strength and the internuclear distance. The latter is accomplished by measuring the REDOR dipolar evolution, $\Delta S/S_0$, as function of dipolar recoupling time, (nT_R), and its subsequent fitting with a simulated curve (6, 7). In addition, the extent of the effect as manifested by the relative size of the difference peak, $\Delta S/S_0$, provides a lower limit estimate for the fraction of species experiencing proximity of a particular length scale. These properties of the REDOR experiment are exploited in the manuscript to determine the extent of dispersion of P species within the ACC, and of the interactions of citrate carboxylates with P moieties.

In order to substantiate and expand the REDOR-based geometric characterization and its implications regarding the

molecular arrangements in the gastrolith, simulated REDOR difference curves, $\Delta S/S_0$, as a function of dipolar evolution time were performed. The simulations are shown in Fig. S4 for a representative set of $^{13}C\cdots^{31}P$ distances.

Estimating the concentration of P molecules dispersed within the ACC. The $64T_R$ $^{13}C\{^{31}P\}$ REDOR spectra (Fig. 3) show approximately 50% $\Delta S/S_0$, indicating that at least half of the ACC carbonate carbons are within 9.0 Å from a ^{31}P atom. This is straightforwardly rationalized by visualizing a phosphorous (minor component) surrounded by a "sea" of carbonates (major component), hence resulting in a distribution of $^{31}P\cdots^{13}C$ distances. To fit the experimental data, a simplified model that accounts for the distance distribution was employed. Spheres of $CaCO_3 \cdot H_2O$ with 1:1 ratio and C number density of 12.14 atoms/nm^3 (as for monohydratecalcite having the same stoichiometry) with a ^{31}P at the center, and radii $R = 10$, 9, 8, and 7 Å were analyzed.

$^{13}C\{^{31}P\}$REDOR dipolar evolution resulting from each sphere was calculated according to the following protocol: (*i*) Each sphere was "sliced" to spherical rings, 1.0 Å thick, starting from 3.0 Å (inner radius, r_i, 3 Å); within each spherical ring a single $^{13}C\cdots^{31}P$ distance is assumed for all carbons: $r_i + 0.5$ Å; a single REDOR curve is calculated for each ring. (*ii*) The weight of each ring is given by the volume ratio of the spherical ring to that of the entire sphere, leaving a "hollow" center of 3-Å radius to accommodate a P molecule (with Ca^{2+} and H_2O). The resulting weight is $a^R(r_i) = [(r_i + 1)^3 - r_i^3]/[R^3 - 3^3]$ (values are listed in Table S3). (*iii*) The simulated REDOR $\Delta S/S_0$ evolution from an individual spherical ring was multiplied by the weight. (*iv*) The sum of the individual weighted contributions from all rings ($r_i = 3,\ldots,R - 1$ Å) within a sphere (R) yield the weighted $\Delta S/S_0$ REDOR evolution curves (Fig. 3*D*). Effects that may arise from multiple interactions $^{13}C\cdots^{31}P_n$ are ignored in this model; this is fully justified in the case of spheres with radius $R \geq 7$ Å and maximum dipolar evolution time of 12.8 ms.

The measured $\Delta S/S_0$ REDOR values from two gastroliths are shown in Fig. 3*D*. The experimental data points are contained between the simulated curves of the 9- and 8-Å spheres, indicating that, on average, within each sphere of 8- to 9-Å radius, a P molecule is present. This finding translates to a concentration of 3–4 P/Ca mol % within the ACC.

Geometric implications for citrate interactions. The relatively small abundance of the citrate compared to the carbonates (1.3–5.2 citrate/Ca mol %) results in S/N that prevents detailed analysis as done for the carbonates. Therefore, conclusions are drawn based on the analysis of the $\Delta S/S_0 \sim 0.75 \pm 0.10$ observed for citrate carboxylate at the longest dipolar recoupling time 12.8 ms. The two types of carboxylates (*1* and *4*) are not resolved and are treated as identical (182 ppm, Fig. 1).

The observed $\Delta S/S_0$ is geometrically interpreted between the following two limiting descriptions: (*i*) All citrate carboxylates have similar average pairwise $^{13}C\cdots^{31}P$ distance; in such a case each carboxylate carbon is 5.0 Å from a P atom. This distance is determined from finding the REDOR curve that crosses $\Delta S/S_0 \sim 0.75$ at 12.8-ms dipolar evolution time (Fig. S4). (*ii*) The 75% REDOR $\Delta S/S_0$ represents 75% of the citrate (carboxylates) that are fully affected, i.e., reach $\Delta S/S_0 \sim 1$. In such a case these carboxylates must be within a distance shorter than 4.5 Å from a P atom; this is seen in Fig. S4 by the 4.5-Å REDOR curve (represents the shortest possible distance with $\Delta S/S_0 = 1$ at 12.8 ms). The implication is that the remaining 25% citrate carboxylates are not closer than 7.5 Å from a P atom ($\Delta S/S_0 \sim 0$ at 12.8 ms dipolar evolution).

Given these close proximities between citrate carboxylates and a P molecule indicated by the REDOR results, the occurrence of a wide distribution of $^{13}C\cdots^{31}P$ distance is ruled out. The emerging description clearly identifies citrate molecules and P-bearing moieties forming molecular arrangement within a narrow range of possible geometries whose chemical implications are described in the main text. We note that the current data cannot exclude/prove the occurrence of proximities to multiple P sites as may occur if citrate is adjacent to a P-rich, apatite-like surface (8–10).

$^{31}P \rightarrow {}^{13}C$ TEDOR (tansferred-echo double resonance) and 2D-HETCOR (heteronuclear correlation) analysis and implications. The 2D-HETCOR employs $24T_R$ (4.8 ms) $^{31}P\{^{13}C\}$ REDOR dipolar recoupling prior and following the coherence transfer (Fig. S5). A $^{31}P\cdots^{13}C$ dipolar evolution will lead to $\Delta S/S_0$ greater than 0.05 for internuclear distance shorter than 6 Å (Fig. S4, 6 Å REDOR curve). This 5% REDOR effect sets the detection limit. Therefore, in this 2D NMR experiment, a cross-peak between carbon and phosphorous implies <6 Å spatial proximity between the two nuclei, meaning between ACC carbonates and Pi, and between ACC carbonates and PEP.

1. Wishart DS, et al. (2009) HMDB: A knowledgebase for the human metabolome. *Nucleic Acids Res* 37:D603–D610.
2. Wishart DS, et al. (2007) HMDB: The human metabolome database. *Nucleic Acids Res* 35:D521–D526.
3. Williams G, Sallis JD (1980) The synthesis of unlabeled and 32P-labeled phosphocitrate and analytical systems for its identification. *Anal Biochem*102:365–373.
4. Kaustov L, et al. (2003) Inhibition mode of a bisubstrate inhibitor of KDO8P synthase: A frequency-selective REDOR solid-state and solution NMR characterization. *J Am Chem Soc* 125:4662–4669.
5. Kaustov L, et al. (2000) Structural and mechanistic investigation of 3-deoxy-D-manno-octulosonate-8-phosphate synthase by solid-state REDOR NMR. *Biochemistry* 39:14865–14876.
6. Mehta AK, Shayo Y, Vankayalapati H, Hurley LH, Schaefer J (2004) Structure of a quinobenzoxazine-g-quadruplex complex by REDOR NMR. *Biochemistry* 43:11953–11958.
7. Paik Y, et al. (2007) Rotational-echo double-resonance NMR distance measurements for the tubulin-bound paclitaxel conformation. *J Am Chem Soc* 129:361–370.
8. Ndao M, et al. (2009) A $^{13}C\{^{31}P\}$ REDOR NMR investigation of the role of glutamic acid residues in statherin- hydroxyapatite recognition. *Langmuir* 25:12136–12143.
9. Bertmer M, Eckert H (1999) Dephasing of spin echoes by multiple heteronuclear dipolar interactions in rotational echo double resonance NMR experiments. *Solid State Nucl Magn Reson* 15:139–152.
10. Hu Y, Rawal A, Schmidt-Rohr K (2010) Strongly bound citrate stabilizes the apatite nanocrystals in bone. *Proc Natl Acad Sci USA* 107:22425–22429.

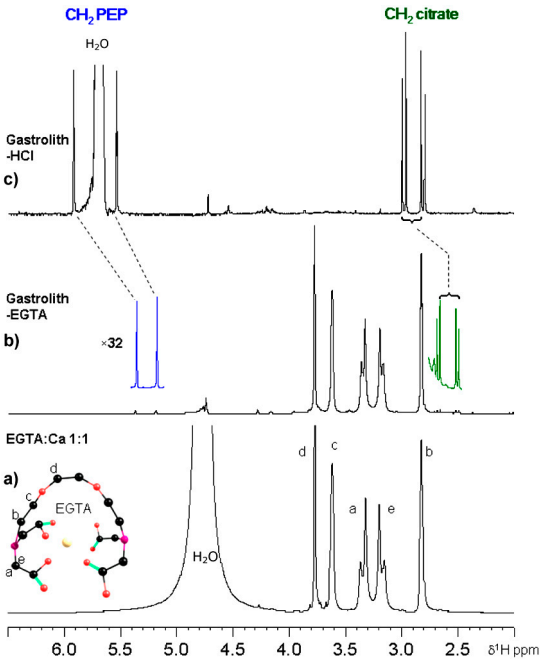

Fig. S1. ^{1}H solution NMR spectra of (*a*) EGTA : Ca^{2+}, (*b*) gastrolith-EGTA, (*c*) gastrolith-HCl. The experimental parameters of all the solution NMR measurements are reported in Table S4.

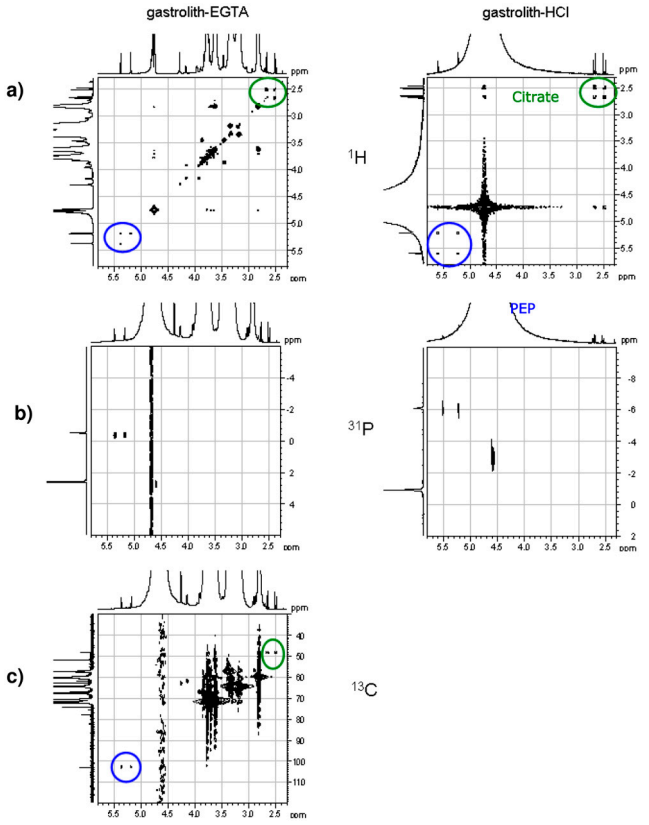

Fig. S2. (*a*) The ^{1}H-^{1}H correlation (COSY) spectra of gastrolith-EGTA (*Left*) and gastrolith-HCl (*Right*) show the geminally coupled proton pair of PEP circled in blue, and the AB pair of citrate circled in green. The intense peaks (*Left*) are from EGTA. Neither proton pair exhibits any additional ^{1}H correlations. Both the 1D projections and the 2D spectra were acquired with water suppression (4.7 ppm). (*b*) The ^{1}H-^{31}P HMBC spectra reveal a long-range J coupling only between the two geminally coupled protons (vinylic) and the more shielded (0.06 ppm) phosphate $^{4}J_{HP} \sim 1.1$ Hz), in accordance with its assignment as PEP. This spectrum therefore identifies the major phospho-organic molecule within the gastrolith soluble fraction as PEP. (*c*) The ^{1}H-^{13}C HSQC spectrum reveals a short-range J coupling between the two geminally coupled protons (vinylic) and the 102.9 ppm C_3 carbon of PEP, and between the AB protons and citrate C_2 at 48.3 ppm. This spectrum therefore solidifies the PEP and citrate assignments as the major organic molecules within the gastrolith soluble fraction.

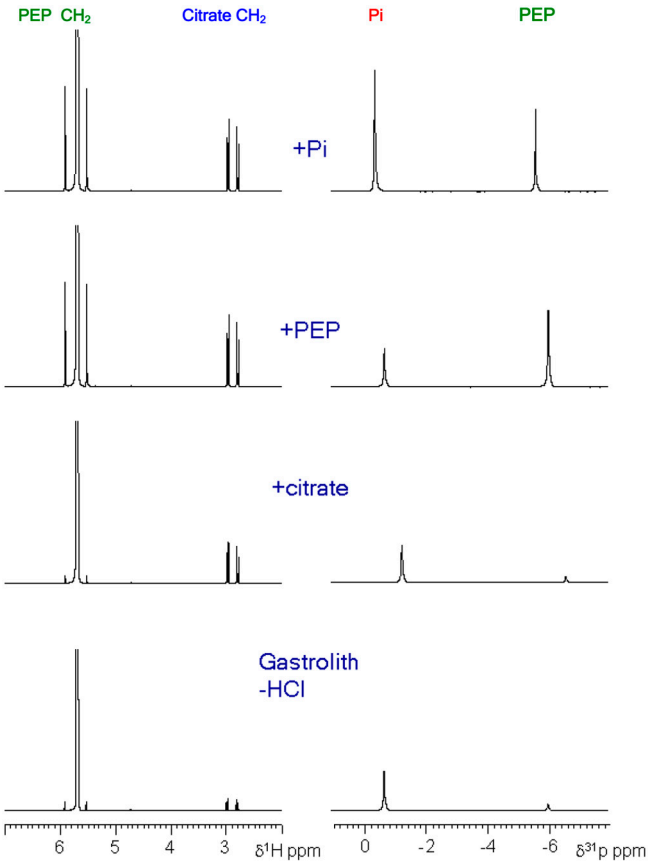

Fig. S3. ^{1}H and ^{31}P solution NMR spectra of the gastrolith-HCl solution, followed by stepwise addition of citric acid, PEP, and Pi. The final spectra (*Top*) were referenced by addition of 2,2-dimethyl-2-silapentane-5-sulfonate to the NMR tube. A series of sample spiking experiments within a single NMR tube were conducted to confirm the identification of PEP, citric acid, and Pi as the major species in the gastrolith soluble fraction. The ^{1}H (*Left*) and ^{31}P (*Right*) spectra shown are for the gastrolith-HCl solutions (in HOD). (*a*) Gastrolith-HCl solution. (*b*) Addition of citric acid (powder) leads to increase of citrate CH_2 (^{1}H). (*c*) Addition of PEP (powder) results in increase of PEP's CH_2 (^{1}H) peak and P peak. (*d*) Addition of phosphoric acid leads to increase of Pi peak.

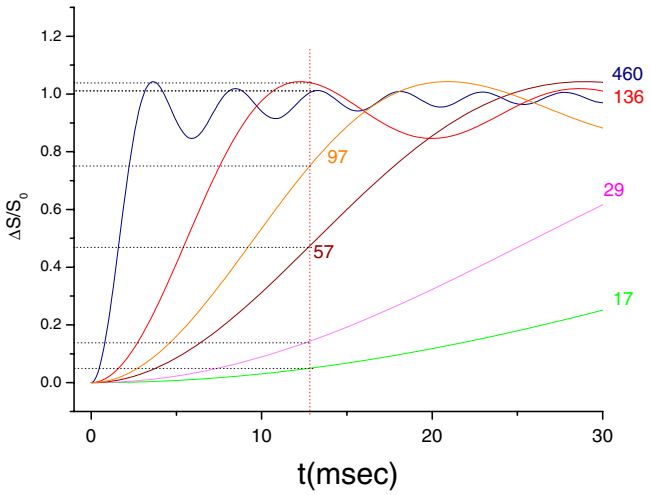

Fig. S4. Simulated ^{13}C{^{31}P} REDOR evolution of $\Delta S/S_0$ for a select set of representative ^{31}P···^{13}C internuclear distances of 3.0, 4.5, 5.0, 6.0, 7.5, and 9.0 Å, and respective dipolar coupling strengths, ν_D, of 460, 136, 97, 57, 29, and 17 Hz.

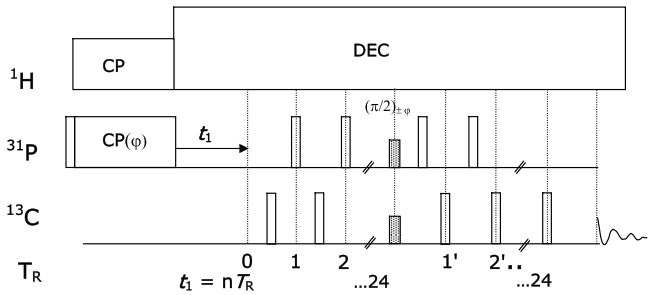

Fig. S5. Graphic representation of the $^{31}P \rightarrow {}^{13}C$ 2D-HETCOR pulse sequence with a TEDOR mixing period.

Table S1. Chemical shifts and ^{1}H-^{1}H J coupling of PEP and citrate and sample pH

	PEP CH_2	Citrate CH_2	Range of pH
Gastrolith-EGTA	5.19, 5.37 ppm $^{2}J_{HH} \sim {}^{4}J_{HP} \sim 1.1$ Hz	2.67, 2.51 ppm $^{3}J_{HH} = 15.66$ Hz	7.5 ± 0.5
Gastrolith-HCl	5.54, 5.92 ppm $^{2}J_{HH} \sim {}^{4}J_{HP} \sim 2.5$ Hz	2.82, 2.98 ppm $^{3}J_{HH} = 16.57$ Hz	2.5 ± 0.5

Under the acidic conditions of the gastrolith-HCl solution PEP and citrate peaks are deshielded relative to the neutral-basic conditions of the gastrolith-EGTA solution.

Table S2. Mol % ratios between the different components within nine gastroliths

Gastrolith	Pi/Ca	PEP/Ca	Citrate/Ca	PEP/Pi	Citrate/PEP	Citrate/Pi
#1	5.2	3.4		68.0		
#2	9.0	2.4	2.0	27.0	76.0	21.3
#3	9.4	2.6	1.3	28.0	52.6	14.8
#4	16.0	2.2	2.3	14.1	97.0	13.7
#5	3.8	2.6	2.0	71.0	76.0	54.0
#6	4.5	2.1	1.8	45.0	87.0	40.0
#7	6.2	0.0	5.2	—	—	84.3
#8	3.4	0.0	3.1	—	—	89.2
#9	12.3	0.0	2.7	—	—	21.8

Table S3. Fractional volumes of spherical rings within four sphere sizes

	Fractional volumes of spherical rings: $a^{R}(r_i)$			
Sphere radius, R, Å	7	8	9	10
Spherical ring r_i, Å				
3–4	0.117089	0.076289	0.052707	0.038027
4–5	0.193038	0.125773	0.086895	0.062693
5–6	0.287975	0.187629	0.12963	0.093525
6–7	0.401899	0.261856	0.180912	0.130524
7–8		0.348454	0.240741	0.17369
8–9			0.309117	0.223022
9–10				0.27852
Total number of carbons in sphere	16.44	25	36	50

Table S4. Experimental NMR parameters for spectra in Figs. S1–S3

Sample	Bruker pulse program	^{1}H ν_0, MHz	^{1}H $\pi/2$ pulse, μs	Presat field, Hz	TD	SW, ppm	NS	DS	D1, s
Fig. S1 (1D ^{1}H)*									
EGTA:Ca^{2+}	zg30	400	11.50		64 k	20.5385	16	2	1
Gastrolith-HCl	zgcppr	600	74.45	5	64 k	11.9622	8	0	3
Gastrolith-EGTA	noesypr1d	600	16.90	13	64 k	16.0109	64	2	3
Fig. S2*a*† (2D ^{1}H-^{1}H)									
Gastrolith-EGTA	cosygppsqf	600	17.0	8	128 × 2 k	6,6	2	16	2.00
Gastrolith-HCl	cosygpqf	400	11.5	8	128 × 2 k	5.14,5.14	1	8	1.41
Fig. S2*b*† (2D ^{1}H-^{31}P)			$\pi/2$ pulse ^{1}H ^{31}P, μs	gradient ratio					
Gastrolith-EGTA	hmbcgpndqf	600	18.5 13.0	12.34:12.34:10.00	128 × 2 k	12, 30	8	16	1.5
Gastrolith-HCl	hmbcgpndqf	400	11.5 8.75		256 × 4 k	6, 200	4	16	1.6
Figure S2*c*§ (2D ^{1}H-^{13}C)			$\pi/2$ pulse ^{1}H ^{13}C, μs						
Gastrolith-EGTA	hsqcetgpsisp (6, 7) 2D ^{1}H-^{13}C	600	18.5 8.5	80:20.10:11: − 5.	128 × 2 k	12, 170	32	16	1.6
Gastrolith-EGTA	1D F1 projectionpower gate	600	8.5		6 k	250.8113	10 k	0	4.0
Fig. S3§ spiking experiments									
^{1}H	zgcppr	600	74.45	5 Hz	64 k	11.9622	8	0	3
^{31}P	zgcppr	600	25.00		32 k	40.5931	64	0	3

*Spectra were acquired with variations on the presaturation method (noesy-presaturation with a 150-ms mixing time) (1) or with composite $\pi/2$ pulses (2, 3) without gradients.

†Spectra used magnitude mode, gradient enhanced, COSY-45 with either off- or on-resonance presaturation during the repetition delay to reduce the HOD contribution. Data processing used linear prediction, SINE window function, and 2-k zero filling in the indirect dimension.

‡Spectra used magnitude mode pulsed field gradient HMBC (4, 5). Data processing used forward linear prediction, QSIN function, zero filling to 1 k in the indirect dimension.

§Data processing of the 2D spectrum used forward linear prediction, QSIN function, zero filling to 1 k in the indirect dimension.

1. Neuhaus D, Ismail IM, Chung CW (1996) "FLIPSY"—A new solvent-suppression sequence for nonexchanging solutes offering improved integral accuracy relative to 1D NOESY. *J Magn Reson Ser A* 118:256–263.
2. Tate S, Inagaki F (1992) Reduction of the water hump using a composite refocusing pulse. *J Magn Reson* 96:635–643.
3. BAX A (1985) A spatially selective composite 90° radiofrequency pulse. *J Magn Reson* 65:142–145.
4. Hurd RE, John BK (1991) Gradient-enhanced proton-detected heteronuclear multiple-quantum coherence spectroscopy. *J Magn Reson* 91:648–653.
5. Parella T, Sanchezferrando F, Virgili A (1995) Purge scheme for efficient suppression of direct responses in gradient-enhanced HMBC spectra. *J Magn Reson A* 112:241–245.
6. Kay L, Keifer P, Saarinen T (1992) Pure absorption gradient enhanced heteronuclear single quantum correlation spectroscopy with improved sensitivity. *J Am Chem Soc* 114:10663–10665.
7. Schleucher J, et al. (1994) A general enhancement scheme in heteronuclear multidimensional NMR employing pulsed field gradients. *J Biomol NMR* 4:301–306.